

SUPPORTING INFORMATION

Twisted MoSe₂ Bilayers with Variable Local Stacking and Interlayer Coupling Revealed by Low-Frequency Raman Spectroscopy

Alexander A. Puretzky,^{*,†,¶} Liangbo Liang,^{†,¶} Xufan Li,[†] Kai Xiao,[†] Bobby G. Sumpter,^{†,§} Vincent Meunier,[‡] and David B. Geohegan[†]

[†]Center for Nanophase Materials Sciences, Oak Ridge National Laboratory, Oak Ridge, Tennessee 37831, United States, [‡]Department of Physics, Applied Physics, and Astronomy, Rensselaer Polytechnic Institute, Troy, New York 12180, United States, [§]Computer Science and Mathematics Division, Oak Ridge National Laboratory, Oak Ridge, Tennessee 37831, United States

[¶]These authors contributed equally to this work.

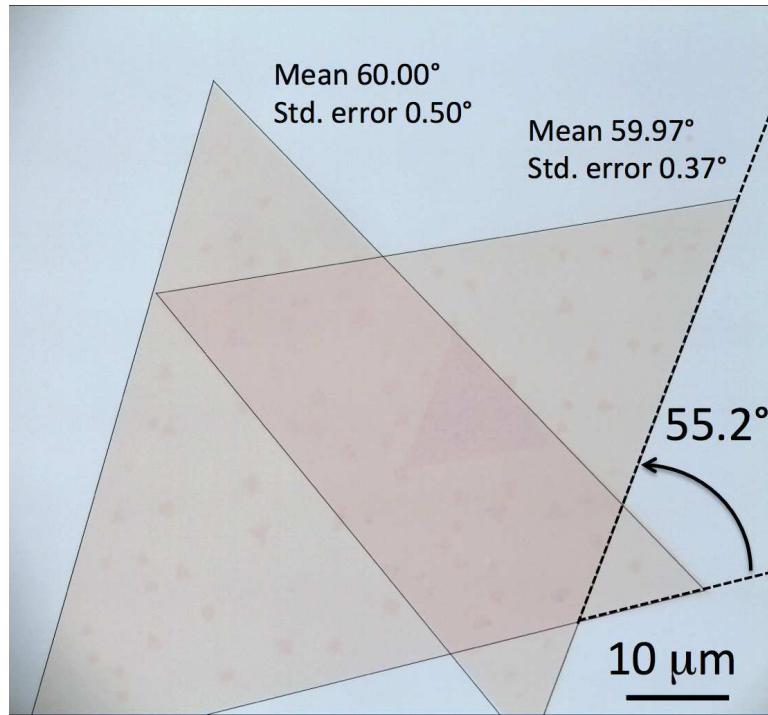


Figure S1. An optical microscope image of a typical MoSe₂ bilayer crystal demonstrating perfect equilateral triangular shape of its as-grown and stacked monolayer components with all three angles equal to $60.0 \pm 0.5^\circ$ and $60 \pm 0.4^\circ$ for the left and right MoSe₂ monolayer components, respectively. The perfect symmetry of the as-grown and transferred MoSe₂ monolayer crystals allows precise determination of the twist angles using optical images. In the shown example the twist angle is equal to $55.2 \pm 0.5^\circ$.

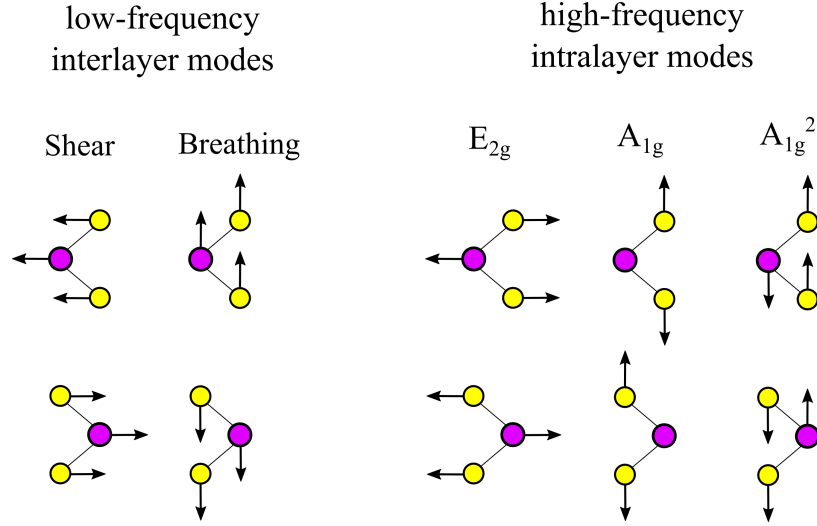


Figure S2. A schematic representation of low-frequency interlayer and high-frequency intralayer Raman modes for bilayer MoSe₂. The black arrows indicate vibrational directions. Low-frequency interlayer Raman modes include in-plane shear and out-of-plane breathing modes, while the high-frequency intralayer Raman modes include E_{2g} and A_{1g} modes. The shear mode has the same symmetry as the E_{2g} mode, and the breathing mode has the same symmetry as the A_{1g} mode. E_{2g} and A_{1g} are the two characteristic Raman peaks in MoSe₂, but the E_{2g} peak is usually very weak or even non-detectable. A_{1g}² is another Raman mode with A_{1g} symmetry but generally with much lower intensity than the A_{1g} peak. Note that strictly speaking, the symmetry assignment here is valid for the natural bulk 2H stacking shown in the schematic. For other high-symmetry stacking configurations and particularly disordered stacking at twist angles, the group symmetry of the bilayer system can be changed, so can the symmetry assignment of Raman modes. In spite of the symmetry change, the vibrational pattern of each Raman mode is essentially the same as the one shown in the schematic. For simplicity and consistency, the notations of E_{2g} and A_{1g} are used for all twisted bilayer systems.

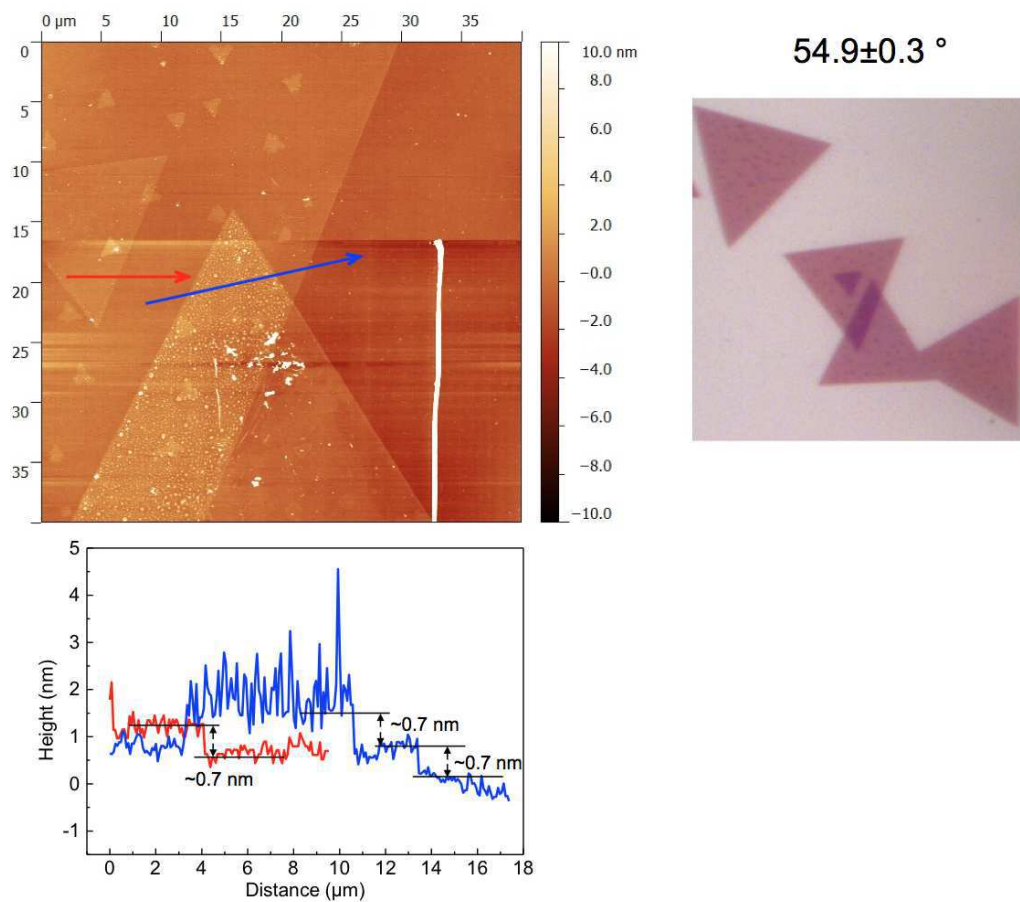


Figure S3. AFM (top left) and optical (top right) images of overlapping MoSe₂ monolayers with the twist angle of $54.9 \pm 0.3^\circ$. The corresponding height profiles along the blue and red arrows are shown at the bottom.

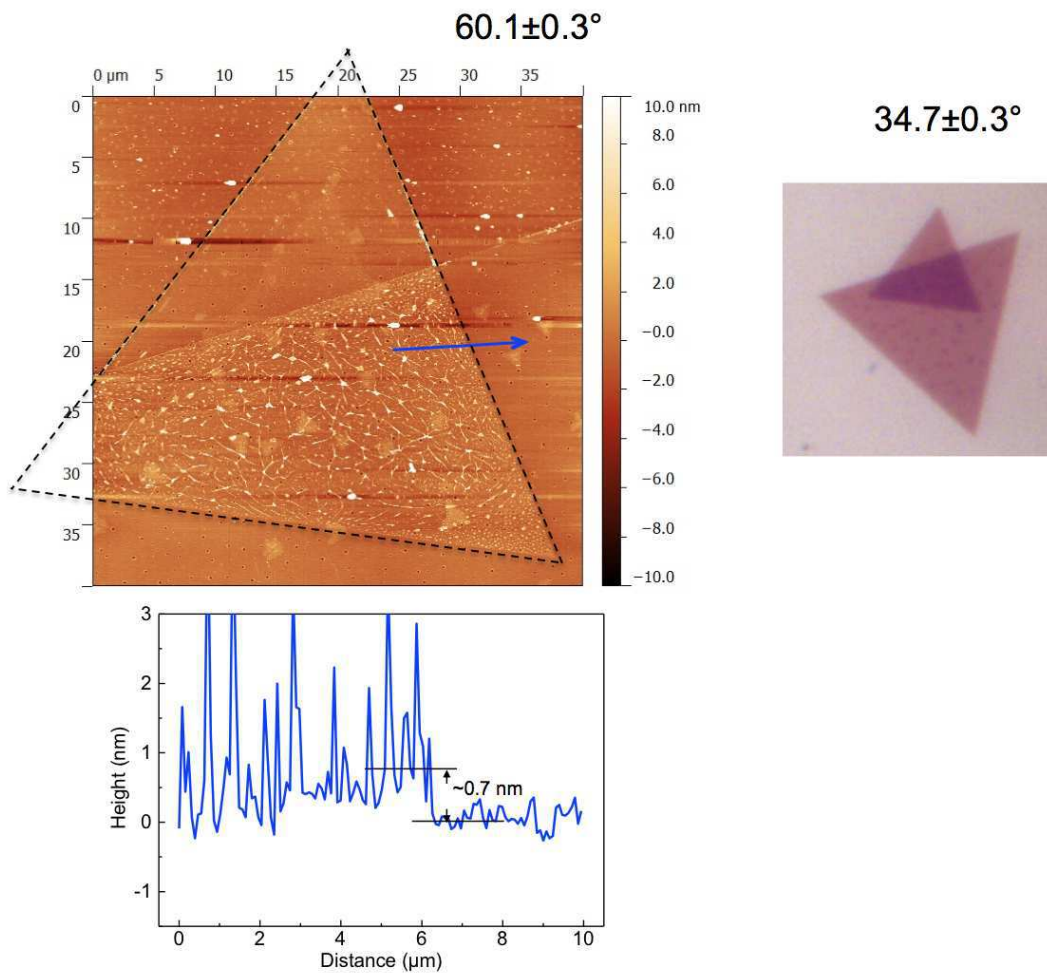


Figure S4. AFM (top left) and optical (top right) images of overlapping MoSe₂ monolayers with the twist angle of $34.7 \pm 0.3^\circ$. The corresponding height profile along the blue arrow is shown at the bottom. The spikes in the line profile indicate multiple-wrinkle morphology in the overlapping region.

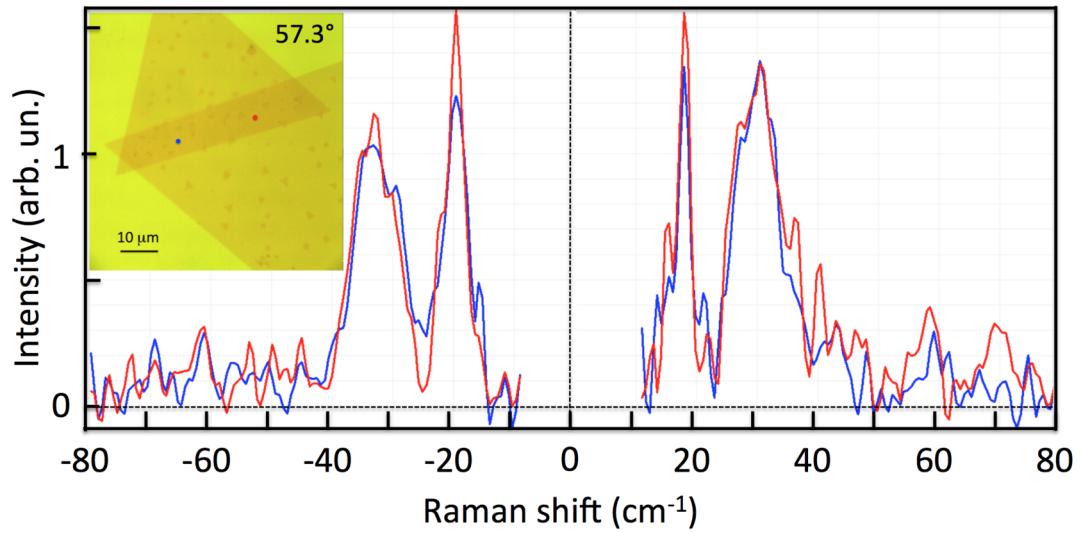


Figure S5. Comparison of LF Raman spectra acquired at different spots of a bilayer with a twist angle of 57.3°. The blue and red dots on the optical image shown in the inset correspond to the positions where the LF Raman spectra presented by the blue and red curves were recorded, respectively.

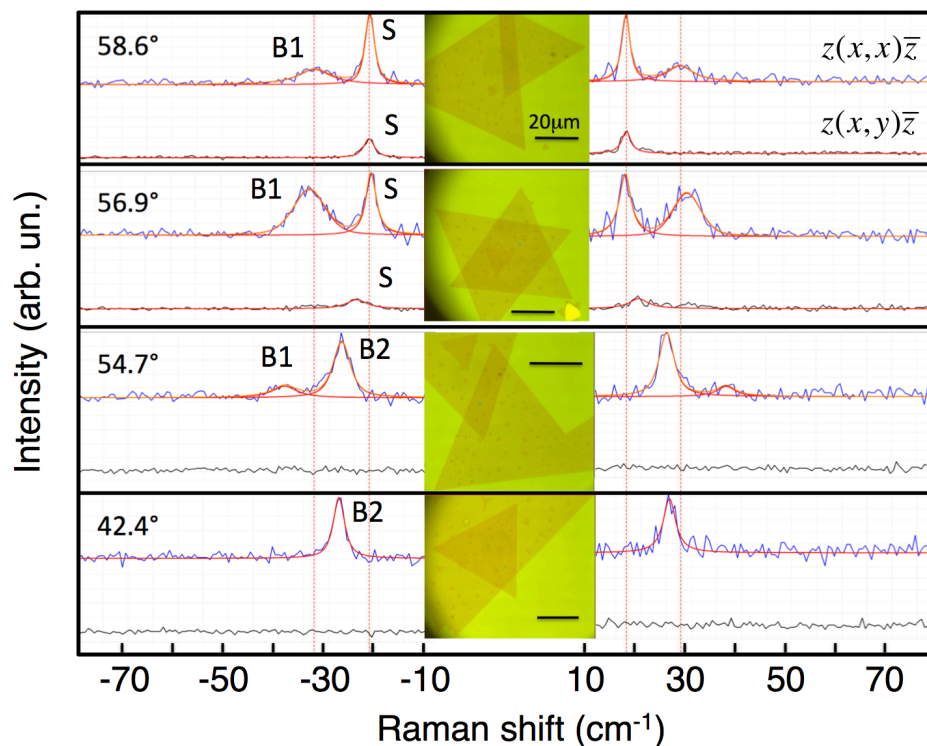


Figure S6. Polarized Raman measurements of the LF shear and breathing modes for four different twist angles. For each twist angle the upper and lower traces are measured using $z(x,x)\bar{z}$ and $z(x,y)\bar{z}$ laser polarization configurations, respectively. The left and the right panels show anti-Stokes and Stokes Raman spectra, respectively. The optical images in the middle show the corresponding MoSe₂ bilayers. For example, both Raman peaks for 54.7° twist angle can be attributed to the breathing modes since they disappear under $z(x,y)\bar{z}$ polarization configuration. Here S, B1, and B2 mark the shear and the two breathing modes, respectively.

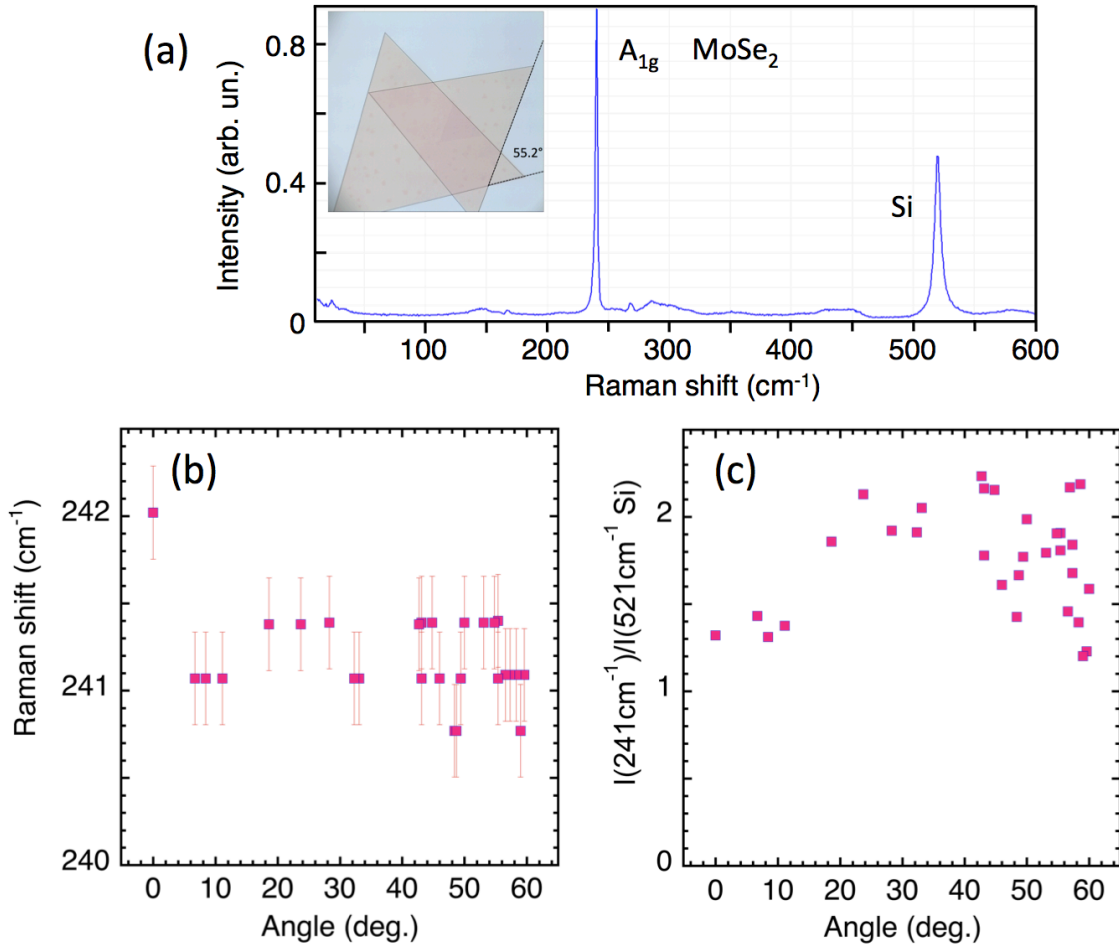


Figure S7. (a) A Raman spectrum of MoSe₂ bilayer with a twist angle of 55.2° measured in the spectral range from 10 to 600 cm⁻¹. The inset shows an optical microscope image of the stamped MoSe₂ monolayers. (b) Frequency of the high-frequency A_{1g} Raman peak versus the twist angle. (c) Peak intensity of the A_{1g} Raman line versus the twist angle. The A_{1g} peak intensity is normalized to the peak intensity of the Si line at 520.7 cm⁻¹.

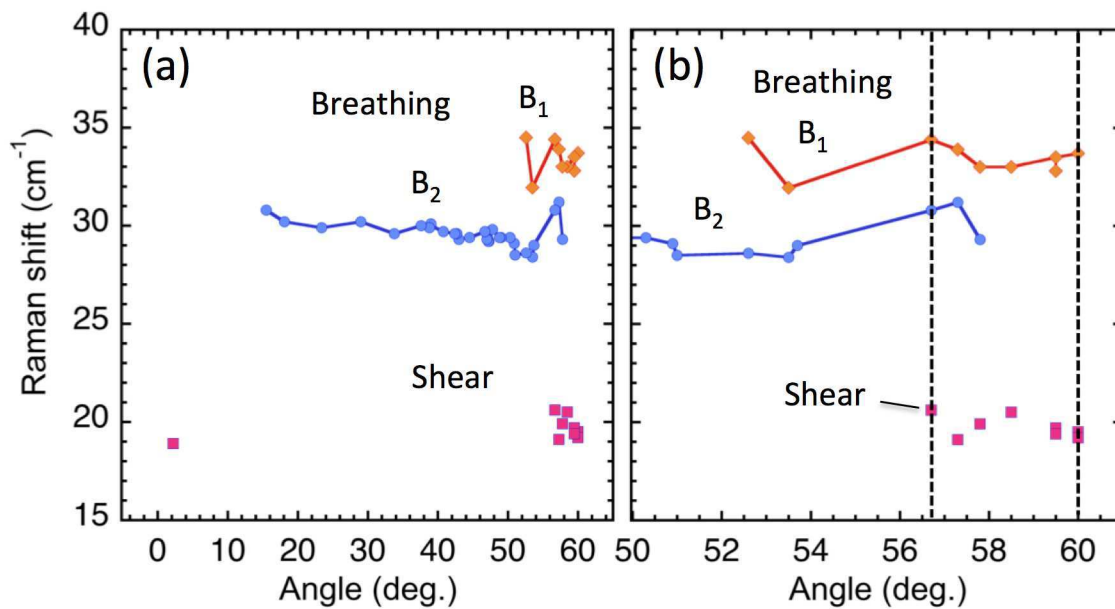


Figure S8. (a) Measured Raman shifts of the shear and two breathing modes, B₁ and B₂ versus a twist angle between two MoSe₂ monolayers doped with W with (b) showing the enlarged region around 60°. The vertical dashed lines mark the twist angle region where the shear Raman line is observed.

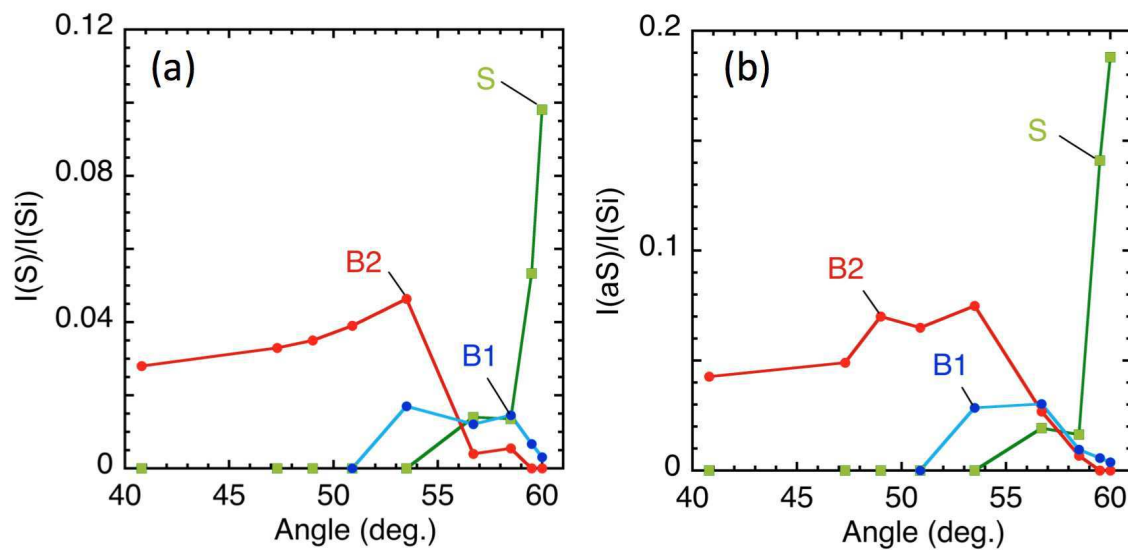


Figure S9. Peak intensities of the shear (S) and two breathing (B₁, B₂) modes normalized to 521cm^{-1} Si peak intensity versus a twist angle for Stokes (a) and anti-Stokes (b) spectral regions measured for MoSe₂ bilayers doped with W.

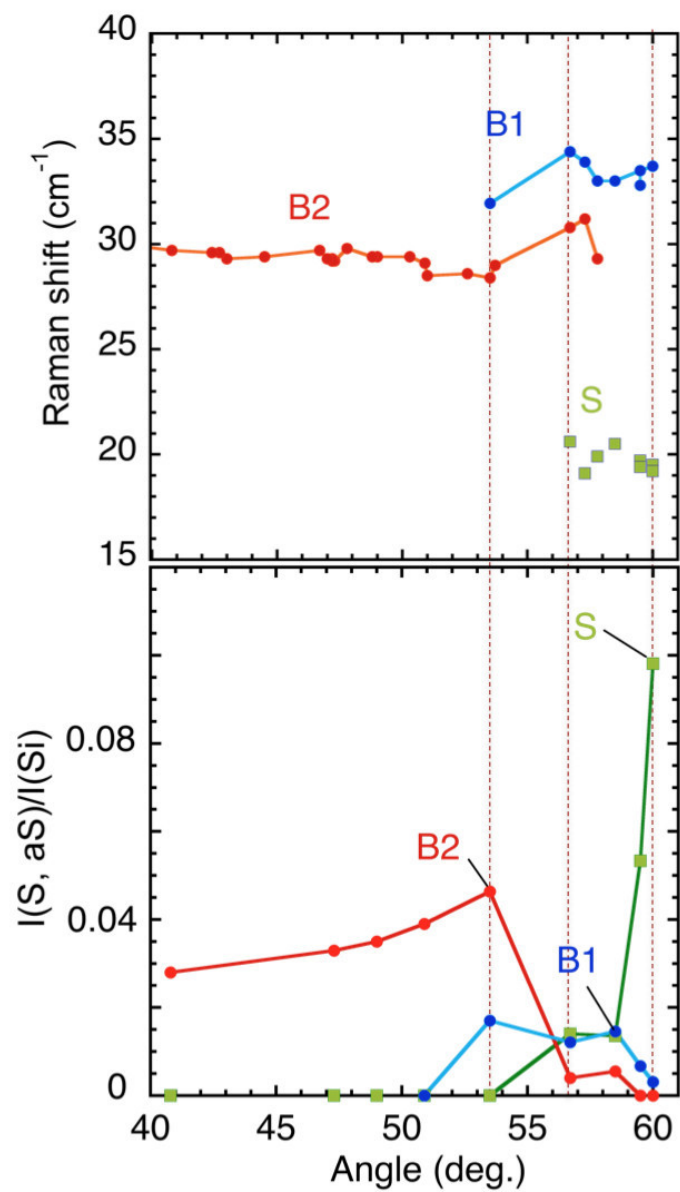


Figure S10. Direct comparison of the Raman shifts (top) and the peak intensities (bottom) versus twist angle for the shear and two breathing modes in the case of W doped MoSe_2 bilayers

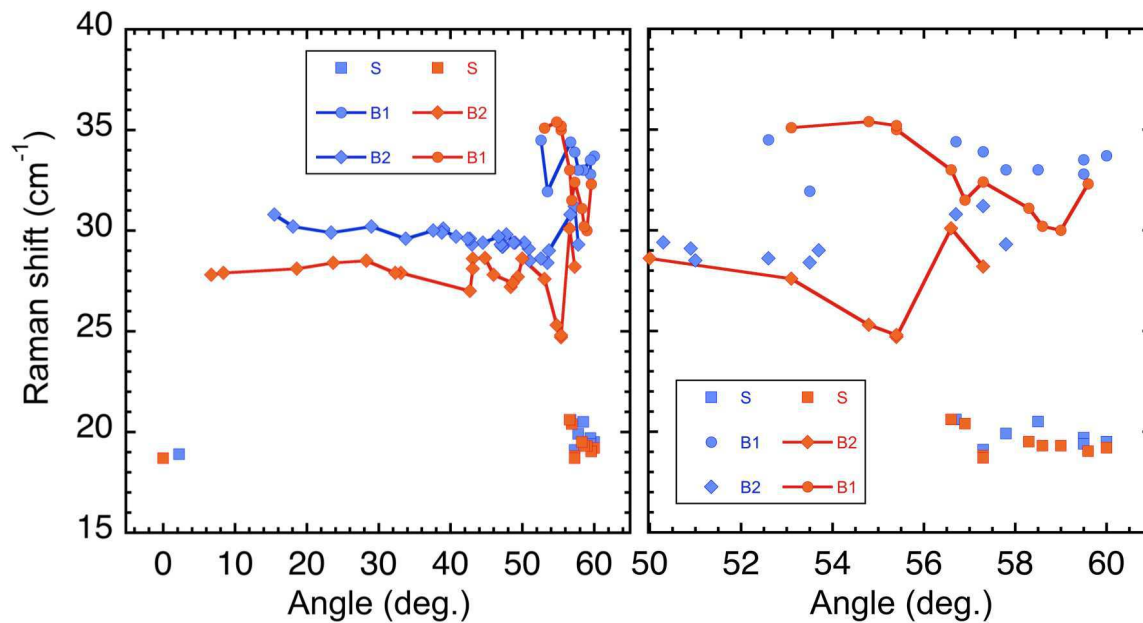


Figure S11. Comparison of the twist angle dependence of the shear and breathing mode frequencies for the pure (sample 1, red symbols) and W doped (sample 2, blue symbols) MoSe₂ bilayers.

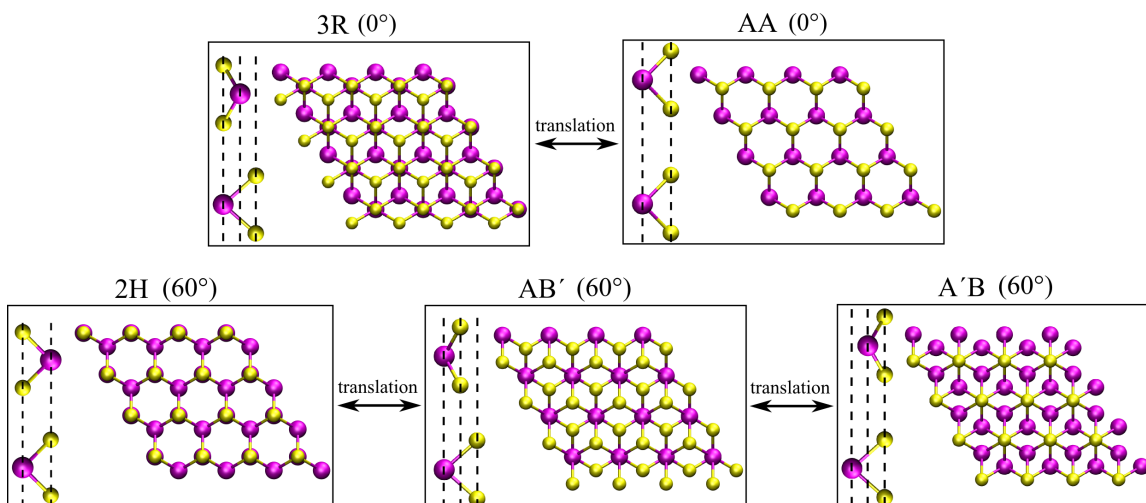


Figure S12. Side and top views of five high-symmetry stacking patterns at 0° and 60° . Purple (yellow) balls correspond to Mo (Se) atoms. At 0° , there are two high-symmetry stacking patterns 3R and AA: for 3R (also denoted as AB), Mo over Se and the other Mo and Se over the center of the hexagons; for AA, Mo over Mo and Se over Se. Both stacking configurations are interchangeable by in-plane translation. At 60° , there are three high-symmetry stacking patterns 2H, AB' and A'B: for 2H (also denoted as AA'), Mo over Se and Se over Mo; for AB', Mo over Mo and all Se over the center of the hexagons; for A'B, Se over Se and all Mo over the center of the hexagons. All three stackings are interchangeable by in-plane translation as well. In addition, the stackings at 0° and 60° are also interchangeable by 60° rotation, depending on the rotation center. Note that 2H at 60° is the most stable stacking, and 3R at 0° is the second most stable stacking. These two stackings exist in natural and CVD-grown bilayer systems. But in the artificially stacked and twisted bilayer samples in this work, all five stackings are possible. AB' is the third most stable stacking, A'B is the fourth stable stacking, and AA is the least stable stacking.

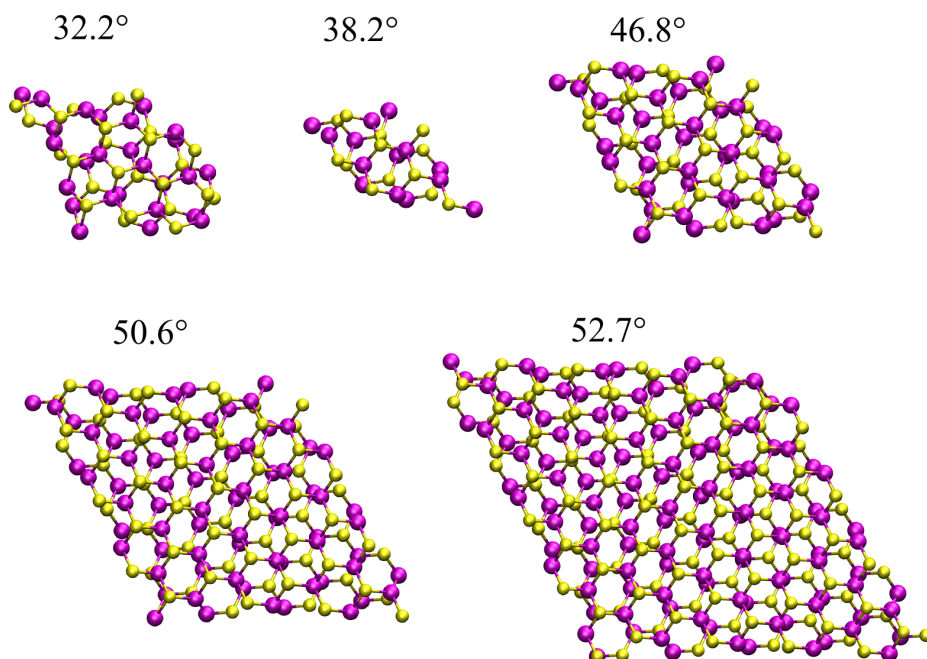


Figure S13. Atomic structures of bilayer MoSe_2 with $\theta \neq 60^\circ$ considered in DFT calculations. They correspond to commensurate bilayer structures (i.e., periodic boundary conditions can be applied in the in-plane directions and a unit cell can be located). Purple (yellow) balls correspond to Mo (Se) atoms. For each twist angle, a unit cell is shown and its size varies strongly with the angle. Note that the twist angles need to be precise up to at least four decimal points in order to locate the highly commensurate bilayer systems. In detail, the twist angles shown here actually correspond to 32.2040° , 38.2132° , 46.8265° , 50.5700° and 52.6590° , respectively. However, for simplicity, they are shortened to one decimal point for discussions throughout the text. In DFT calculations, for 32.2° , the in-plane lattice constants are 11.73 \AA and a $6 \times 6 \times 1$ k-point sampling was used; for 38.2° , the in-plane lattice constants are 8.61 \AA and a $9 \times 9 \times 1$ k-point sampling was used; for 46.8° , the in-plane lattice constants are 14.18 \AA and a $6 \times 6 \times 1$ k-point sampling was used; for 50.6° , the in-plane lattice constants are 19.79 \AA and a $3 \times 3 \times 1$ k-point sampling was used; for 52.7° , the in-plane lattice constants are 25.41 \AA and a $1 \times 1 \times 1$ k-point sampling was used.

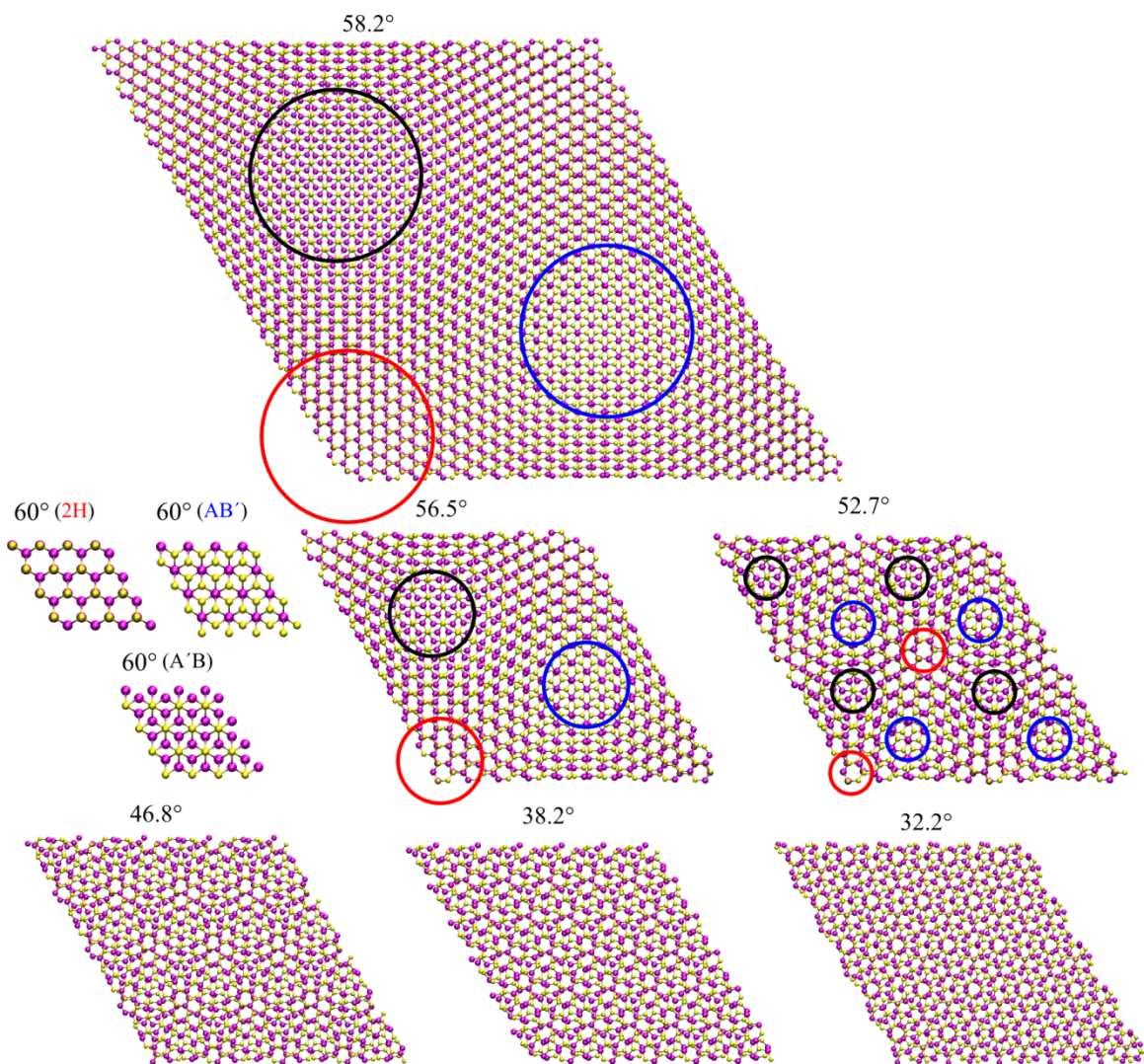


Figure S14. Commensurate bilayer MoSe₂ systems for twist angles above 30° to illustrate how the stacking evolves with the angle. Different sizes of supercell structures are shown here for comparison: 4×4 supercell for 60°, 1×1 supercell for 58.2° and 56.5°, 2×2 supercell for 52.7°, 4×4 supercell for 46.8°, 6×6 supercell for 38.2°, and 5×5 supercell for 32.2°. At 60°, there are three high-symmetry stacking patterns (2H, AB' and A'B): for 2H, Mo over Se and Se over Mo; for AB', Mo over Mo and all Se over the center of the hexagons; for A'B, Se over Se and all Mo over the center of the hexagons. The red, blue and black circles highlight the presence of 2H, AB' and A'B stackings in a twist angle, respectively. Clearly, the more the angle deviates from 60°, the smaller 2H, AB' and A'B stacking areas become. For 32.2°, the stacking becomes completely disordered.

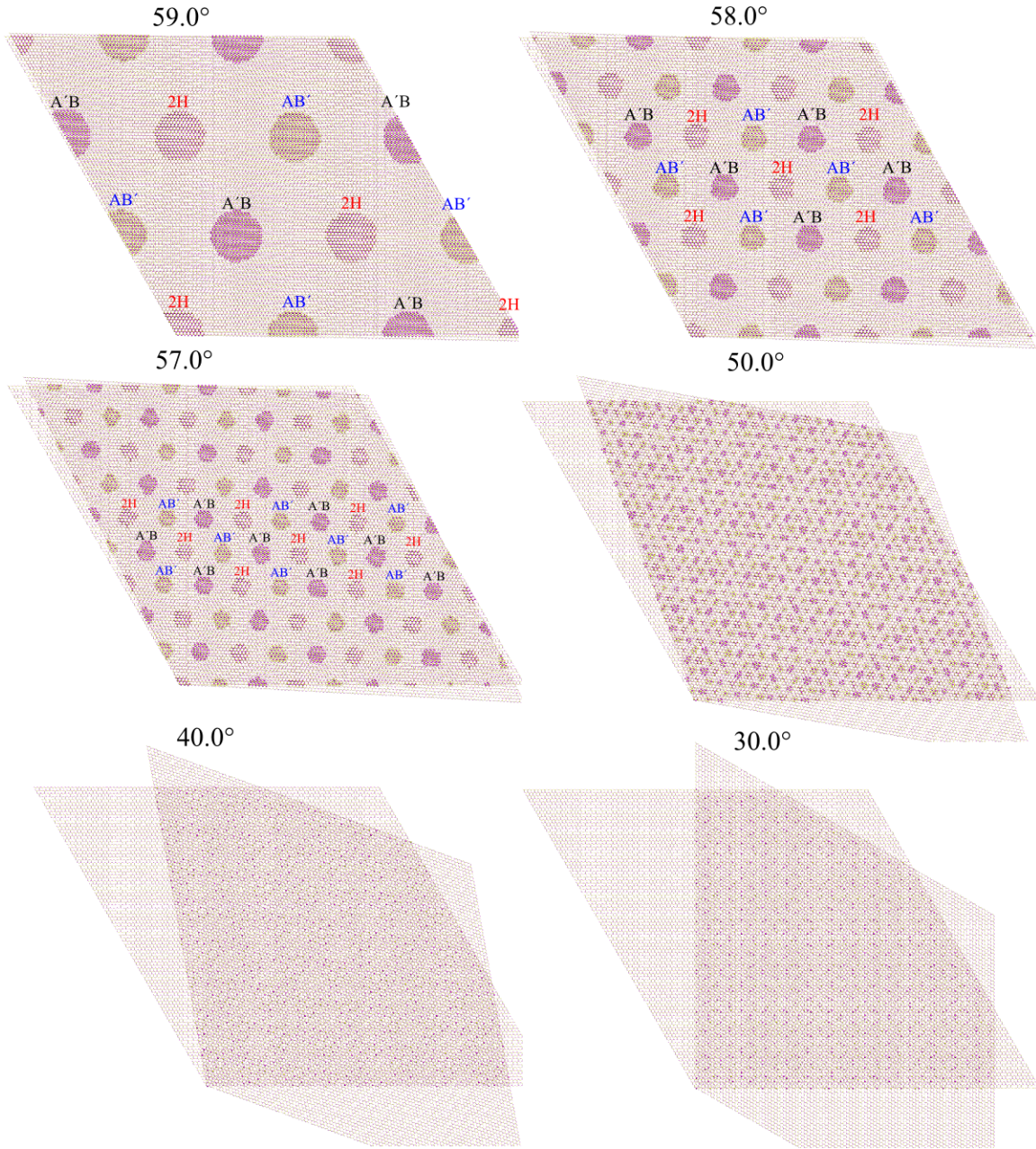


Figure S15. Non-commensurate bilayer MoSe₂ systems for twist angles above 30° to illustrate how the stacking evolves with the angle. First, a primitive unit cell of bilayer MoSe₂ at 2H stacking was chosen to build a 100×100 supercell, which corresponds to 60°. Then with respect to the bottom left corner, the top layer was rotated from 60° to 30°, leading to non-commensurate bilayer systems. Interestingly, when the system is only slightly deviated from 60°, all three high-symmetry stackings 2H, AB' and A'B appear in roughly circular shapes, and the atoms inside the circles are highlighted by larger spherical radii. These circular high-symmetry stacking patches are clearly periodic, similar to the triangular lattice. Their sizes continuously decrease with the angle deviating from 60°. When $\theta < 55^\circ$, the high-symmetry stacking patches begin to disappear and the overall stacking becomes increasingly disordered.

Table S1. For bilayer MoSe₂ at different twist angles, this table shows the DFT calculated average interlayer separation d (in Å), total energy ΔE (in meV/atom), frequency ω (cm⁻¹) and Raman intensity I (arbitrary unit) of interlayer shear mode, interlayer breathing mode, A_{1g} mode. 0° has two high-symmetry stacking patterns 3R and AA, while 60° has three high-symmetry stacking patterns 2H, AB' and A'B. For these stackings, the unit cell is small with 6 atoms and Raman intensities were calculated. For 38.2°, it has the smallest unit cell with 42 atoms among all considered twist angles $\theta \neq 60^\circ$, and Raman intensities were calculated though very time-consuming. “-“ indicates Raman intensities not calculated, as the corresponding systems are too large for costly Raman calculations. Note that for 38.2°, the computed intensities are normalized (i.e., divided by 7) so that they can compare with the values at 60°.

Twist angle	Stacking	d (Å)	ΔE (meV/atom)	Shear mode		Breathing mode		A _{1g} mode	
				ω (cm ⁻¹)	I	ω (cm ⁻¹)	I	ω (cm ⁻¹)	I
0°	3R	6.35	1.0	19.74	0.34	30.19	1.92	245.88	29.39
	AA	7.13	13.7	0.00	0.00	21.48	0.04	245.17	23.90
32.2°	-	6.72	8.5	0.00	-	24.87	-	245.40	-
38.2°	-	6.73	8.5	0.00	0.00	23.38	0.66	245.30	25.30
46.8°	-	6.72	8.5	1.22	-	24.06	-	245.37	-
50.6°	-	6.70	8.4	2.53	-	24.61	-	245.45	-
52.7°	-	6.67	7.5	2.41	-	23.81	-	245.41	-
60°	2H	6.36	0.0	20.12	0.91	32.35	0.44	245.56	26.59
	AB'	6.48	5.6	14.02	0.11	24.68	2.04	245.57	28.22
	A'B	7.06	13.0	0.00	0.00	22.71	0.48	245.26	25.04